Exploring the doubly charged Higgs boson of the left-right symmetric model using vector boson fusionlike events at the LHC

Bhaskar Dutta,[1] Ricardo Eusebi,[1] Yu Gao,[1] Tathagata Ghosh,[1] and Teruki Kamon[1,2]

[1]*Mitchell Institute for Fundamental Physics and Astronomy, Department of Physics and Astronomy, Texas A&M University, College Station, Texas 77843-4242, USA*

[2]*Department of Physics, Kyungpook National University, Daegu 702-701, South Korea*

(Received 20 April 2014; published 15 September 2014)

This paper studies the pair production of the doubly charged Higgs boson of the left-right symmetric model using a multilepton final state in the vector boson fusionlike processes. The study is performed in a framework consistent with the model's correction to the standard model ρ_{EW} parameter. Vector boson fusion topological cuts, the number of leptons, and p_T cuts on the leptons are found to be effective in suppressing the background. Significant mass reach can be achieved for exclusion/discovery of the doubly charged Higgs boson for the upcoming LHC run with a luminosity of $\mathcal{O}(10^3)$ fb^{-1}.

DOI: 10.1103/PhysRevD.90.055015 PACS numbers: 12.60.-i, 12.60.Fr, 13.85.Rm

I. INTRODUCTION

The LHC experiments have successfully discovered the last missing piece of the standard model (SM)—the elusive Higgs boson. However, no sign of any physics beyond the SM has been observed yet. Although the standard model has been extremely effective, many unsolved questions still remain. The left-right (L-R) symmetric model [1–4] provides appealing solutions for some of these questions. First, it explains the origin of the parity violation at the weak scale. In L-R models, parity is an exact symmetry of the weak-interaction Lagrangian at an energy scale much higher than the SM scale. The parity violation arises from the spontaneous symmetry breaking driven by a vacuum not being invariant under parity. Second, the L-R model predicts the existence of right-handed neutrinos that explain the light neutrino mass via the see-saw mechanism. Finally, these models place quarks and leptons on the same footing in the weak interactions and provide a simple formula for the electric charge, involving only the weak isospin and the difference between the baryon and lepton numbers (B-L).

In this paper, we explore the LHC signature of these L-R models by focusing on the like-sign lepton pairs from the decays of the left-handed doubly charged scalars ($\delta_L^{\pm\pm}$). It is worthwhile to mention here that the doubly charged Higgs particles may also arise in other models, such as the Georgi-Machacek model [5], the Littlest Higgs model [6], and 3-3-1 models [7,8]. Recent publications [9–12] have studied the doubly charged Higgs belonging to different multiplets. A rather interesting work [13] has investigated lepton-number-violating decays of heavy flavor fermions (t, τ) induced by the doubly charged Higgs boson.

In Refs. [9,14–25], the production of the doubly charged Higgs boson has been considered using the Drell-Yan (DY) mechanism in the scope of the models described above. In this paper, we consider the production of a pair of doubly charged Higgs bosons accompanied by two energetic tagging jets, predominantly produced by vector boson fusion (VBF) processes, where the leading jets are very helpful to reduce the background. In various different contexts, the single production of a doubly charged Higgs boson through $W^{\pm}W^{\pm}$ fusion at the LHC has been discussed in some earlier studies [25–29]. In these studies the vacuum expectation value (VEV) of the triplet sector is assumed to be nonzero, and consequently the final states with $W^{\pm}W^{\pm}$ are considered using the decay modes of W containing e and μ. However, we differ from these searches in the sense that we have only considered the scenario where the left triplet VEV of L-R symmetric models is zero, to avoid unnatural experimental consequences. In such a scenario, we will consider e, μ, and τ (hadronic) final states arising from the doubly charged Higgs boson decays directly along with two high-p_T jets. By using VBF topological cuts, we shall offer a search strategy of the doubly charged Higgs boson at the LHC, complementary to the current search being performed by CMS [30] and ATLAS [31,32] for multilepton final states without using two tagged jets. The potential discovery of $\delta_L^{\pm\pm}$ in both the VBF and DY channels can be instrumental in determining its electroweak (EW) origin.

The paper is organized as follows: Section II briefly reviews the L-R symmetric model. Section III discusses the production mechanism and the subsequent decay of the doubly charged Higgs. The results for future LHC searches are given in Sec. IV. Finally, the conclusions drawn from the study have been summarized in Sec. V.

II. THE LEFT-RIGHT SYMMETRIC MODEL

Here we present a brief overview of the $SU(2)_L \times SU(2)_R \times U(1)_{B\text{-}L}$ L-R symmetric models [1–4]. The scalar sector of these models consists of the following Higgs multiplets [33–37]:

$$\phi = \begin{pmatrix} \phi_1^0 & \phi_1^+ \\ \phi_2^- & \phi_2^0 \end{pmatrix}, \tag{1}$$

$$\Delta_L = \begin{pmatrix} \delta_L^+/\sqrt{2} & \delta_L^{++} \\ \delta_L^0 & -\delta_L^+/\sqrt{2} \end{pmatrix}, \tag{2}$$

$$\Delta_R = \begin{pmatrix} \delta_R^+/\sqrt{2} & \delta_R^{++} \\ \delta_R^0 & -\delta_R^+/\sqrt{2} \end{pmatrix}. \tag{3}$$

The Higgs mutiplets transform according to $\Delta_L \leftrightarrow \Delta_R$ and $\phi \leftrightarrow \phi^\dagger$. The scalar field potential involving the interactions of ϕ, Δ_L, Δ_R involves numerous parameters. For the reader's convenience, we include the Higgs potenial we have used for our study in Appendix A. Following the notations of Ref. [36], we define

$$\begin{aligned} \rho_{\rm dif} &\equiv \rho_3 - 2(\rho_2 + \rho_1), \\ \Delta\alpha &\equiv (\alpha_2 - \alpha_2')/2. \end{aligned} \tag{4}$$

The VEVs of the bidoublet ϕ and triplets $\Delta_{L,R}$ are given by

$$\langle \phi \rangle = \frac{1}{\sqrt{2}} \begin{pmatrix} \kappa_1 & 0 \\ 0 & \kappa_2 \end{pmatrix}, \tag{5}$$

$$\langle \Delta_{L,R} \rangle = \frac{1}{\sqrt{2}} \begin{pmatrix} 0 & 0 \\ v_{L,R} & 0 \end{pmatrix}. \tag{6}$$

While the bidoublet ϕ breaks the SM symmetry $SU(2)_L \times U(1)_Y \to U(1)_{\rm EM}$, the $SU(2)_R \times U(1)_{B\text{-}L} \to U(1)_Y$ is broken by the triplet VEVs (v_L, v_R) and consequently provides a Majorana mass to the right-handed neutrinos.

A. Vacuum expectation value scenarios

The parameters in the scalar field potential can be severely constrained by various experimental observations. From the K_L-K_S mixing, W_R is constrained to be very heavy ($m_{W_R} > 2.5$ TeV) [38,39]. The gauge invariance of $SU(2)_R \times SU(2)_L \times U(1)_{B\text{-}L}$ requires the coupling of W_R to both Δ_R and ϕ. Consequently, m_{W_R} depends on v_R, κ_1, and κ_2, with both κ_1, κ_2 at the EW scale. Thus, v_R needs to be large ($v_R \gg \kappa_1, \kappa_2$). For simplicity of calculation, we set $\kappa_1 \neq 0$ and $\kappa_2 = 0$.

Thus, after fixing $\kappa_2 = 0$ and $\kappa_1, v_R \neq 0$, there are two options for the left-handed VEV, v_L: (i) $v_L \neq 0$ or (ii) $v_L = 0$. However, v_L is highly constrained to be $v_L \ll \kappa$ by the $\rho_{\rm EW}$ parameter, where $\kappa = \sqrt{\kappa_1^2 + \kappa_2^2}$. For $\kappa_2 = 0$, the $\rho_{\rm EW}$ is given in Ref. [36]:

$$\rho_{\rm EW} \equiv \frac{m_W^2}{\cos^2\theta_W m_Z^2} \simeq \frac{1 + 2v_L^2/\kappa_1^2}{1 + 4v_L^2/\kappa_1^2}. \tag{7}$$

From the experimentally observed value [40] $\rho_{\rm EW} = 1.0004^{+0.0003}_{-0.0004}$ (at 2σ), we obtain a bound $v_L \lesssim 3.5$ GeV, which is very small compared to $\kappa_1 \approx 246$ GeV.

Now, let us take a more detailed look at each left-handed VEV scenario.

1. $v_L \neq 0$

The minimization condition of the Higgs potential in this case sets $\rho_{\rm dif} = 0$. Thus, from the mass spectrum of the left Higgs triplet, presented in Appendix A, we obtain at the tree level

$$m^2_{\delta_L^0} = m^2_{\delta_L^{0*}} = 0. \tag{8}$$

For $m_{\delta_L^0} \ll m_Z$, the Z boson can decay into $\delta_L^0 \delta_L^{0*}$. Since δ_L^0 can only decay to $\nu\nu$ at the tree level, the $Z \to \delta_L^0 \delta_L^{0*}$ decay is invisible, and it becomes constrained by the invisible Z boson decay width measurement. Using Table III in Appendix B, we obtain

$$\Gamma(Z \to \delta_L^0 \delta_L^{0*}) = \frac{g^2 m_Z}{48\pi c_W^2} = 339 \text{ MeV}, \tag{9}$$

which violates the experimental uncertainty on the invisible Z width $\simeq$1.5 MeV [40]. Thus, we can conclude that the $v_L \neq 0$ VEV scenario of L-R symmetric models, with further discrete symmetries imposed, is ruled out. The additional discrete symmetries are discussed in Appendix A.

2. $v_L = 0$

In this scenario, the left-handed Higgs triplet scalars do not mix with their bidoublet counterparts, and they are the mass eigenstates by themselves. $\rho_{\rm dif}$ can be arbitrary in this case. The mass spectrum is given as (see Appendix A for details)

$$\begin{aligned} m^2_{\delta_L^0} &= \frac{1}{2}\rho_{\rm dif} v_R^2, \\ m^2_{\delta_L^+} &= \frac{1}{2}\rho_{\rm dif} v_R^2 + \frac{1}{2}\Delta\alpha\kappa_1^2 = m^2_{\delta_L^0} + \frac{1}{2}\Delta\alpha\kappa_1^2, \\ m^2_{\delta_L^{++}} &= \frac{1}{2}\rho_{\rm dif} v_R^2 + \Delta\alpha\kappa_1^2 = m^2_{\delta_L^0} + \Delta\alpha\kappa_1^2. \end{aligned} \tag{10}$$

We shall see in the subsequent sections that these masses, especially their differences, are of much phenomenological interest.

III. PHENOMENOLOGY AT LHC

In this section, we discuss the VBF production of the doubly charged Higgs boson and its decay channels.

A. Production of the doubly charged Higgs boson

The gauge bosons and the left Higgs triplet couplings can be derived from the corresponding Higgs triplet kinetic term of the Lagrangian,

$$\mathcal{L}_{\rm kin} = (\mathcal{D}_\mu \Delta_L)^\dagger (\mathcal{D}_\mu \Delta_L). \tag{11}$$

The covariant derivative is defined by

$$\mathcal{D}_\mu \Delta_L \equiv i\partial_\mu \Delta_L + \frac{g}{2}\frac{s_W}{c_W} Y B_\mu \Delta_L + \frac{g}{2}[\vec{\tau}.\vec{W}_{L_\mu}, \Delta_L], \tag{12}$$

where $s_W(c_W) = \sin\theta_W(\cos\theta_W)$, with θ_W being the EW mixing angle. The Δ_L has a hypercharge, $Y = 2$. The Feynman rules obtained from Eq. (11) are listed in Table III in Appendix B.

Since $v_L = 0$, those gauge boson–scalar couplings proportional to v_L will vanish. Therefore, the single production of $\delta_L^{\pm\pm}$ by VBF processes is impossible. Instead, we study the production of a pair of doubly charged Higgs, $pp \to \delta_L^{++}\delta_L^{--}jj$. We shall also consider the associated production, $pp \to \delta_L^{\pm\pm}\delta_L^{\mp} jj$, which increases the production cross section by a factor of about 2, as shown in Fig. 2.

VBF processes: In a VBF process, a pair of Higgs triplet scalars $(\delta_L^{\pm\pm}, \delta_L^{\pm})$ is produced by the fusion of two virtual vector bosons (W, Z, γ) radiated by the incoming quarks. Two associated back-to-back "tagging" jets appear in the forward region with a large angular separation $|\Delta\eta_{j_1 j_2}|$.[1] A further kinematic cut on the invariant mass of the two jets $M_{j_1 j_2}$ combined with $|\Delta\eta_{j_1 j_2}|$ will be instrumental in reducing SM backgrounds. Since the pair production of two heavy scalars requires the incoming partons to be very energetic, the tagged VBF jets should also have high p_T. The specific cuts are listed in Sec. IV.

The aforementioned final states can also be produced by DY processes, although the DY production mechanism is not accompanied by the forward-backward jets. Reference [9] made a comparison between the DY and VBF production and found that the VBF cross section is ∼5%–10% of the DY cross section for triplet scalar masses below 1 TeV. Nevertheless, the production of $\delta_L^{\pm\pm}$ by VBF processes and its subsequent discovery is of utmost importance. From the DY production of $\delta_L^{\pm\pm}$, one cannot determine its origin. If the interaction of the left Higgs triplet with the W boson is absent in the Lagrangian in Eq. (12), then two-photon fusion will be the dominant mechanism for the pair production of $\delta_L^{\pm\pm}$ by VBF processes. Hence, the correlation between VBF and DY cross sections will be different from that which would be found if W couplings were present. Consequently, the discovery of $\delta_L^{\pm\pm}$ by means of VBF topological cuts, together with their detection in the DY channel, will shed light on their EW origin.

With this background, let us revisit the mass spectrum of the left Higgs triplet in the VEV scenario under consideration. The mass splitting $\Delta m = m_{\delta_L^{++}} - m_{\delta_L^{+}}$ can enhance the VBF cross section in the t-channel $\delta_L^{\pm}$ exchange, as shown in Fig. 2. However, this mass difference is also subject to $\rho_{\rm EW}$ constraint via the triplet Higgs' contribution to the $W^{\pm}$ boson mass at loop order, as given in Ref. [36]:

$$\Delta\rho_{\rm EW} = \frac{2g^2}{64\pi^2 m_W^2}[f(m_{\delta_L^0}, m_{\delta_L^+}) + f(m_{\delta_L^+}, m_{\delta_L^{++}})], \tag{13}$$

where

$$f(x,y) \equiv x^2 + y^2 - \frac{2x^2y^2}{x^2 - y^2}\ln\left(\frac{x^2}{y^2}\right). \tag{14}$$

We recall the fact that the latest experimental value of $\rho_{\rm EW} = 1.0004^{+0.0003}_{-0.0004}$ [40] allows us to have $\Delta\rho_{\rm EW} \lesssim 0.001$ at 2σ. This yields a severe bound of $\Delta m_{\rm max} \sim 40$ GeV. The bound on the mass splitting as a function of $m_{\delta_L^0}$ and $\Delta\alpha$ has been presented in Fig. 1. This bound also applies for the mass splitting between δ_L^+ and δ_L^0. It is worthwhile to mention here that a bound on $\Delta\alpha$ may arise from the mass bounds on the FCNC scalars [36]. For a fixed $\Delta\alpha$ and Δm we can set an upper bound on the mass of δ_L^0. The dependence of the cross section on Δm is illustrated in Fig. 2. Here we have plotted the variation of the cross section as a function of $m_{\delta_L^{++}}$ for $\Delta m = 0$ and 40 cases.

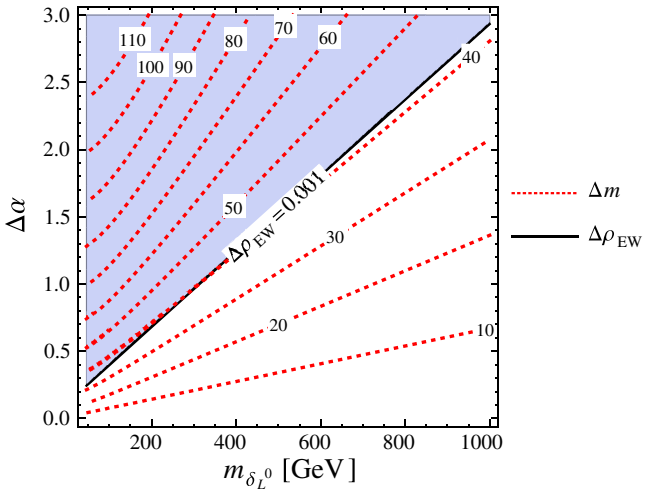

FIG. 1 (color online). Same-value Δm contours (dashed) as a function of $m_{\delta_L^0}$ and $\delta\alpha$, where $\Delta m = m_{\delta_L^{++}} - m_{\delta_L^+}$. The constraint $\Delta\rho_{\rm EW} = 0.001$ is shown by the black thick line. The shaded region is excluded.

[1]Throughout this paper, $j_1 j_2$ in the subscript denotes the dijet pair with the highest invariant mass among all possible pairs of jets in the final state. The tagged dijet pairs are sorted among themselves with respect to their p_T.

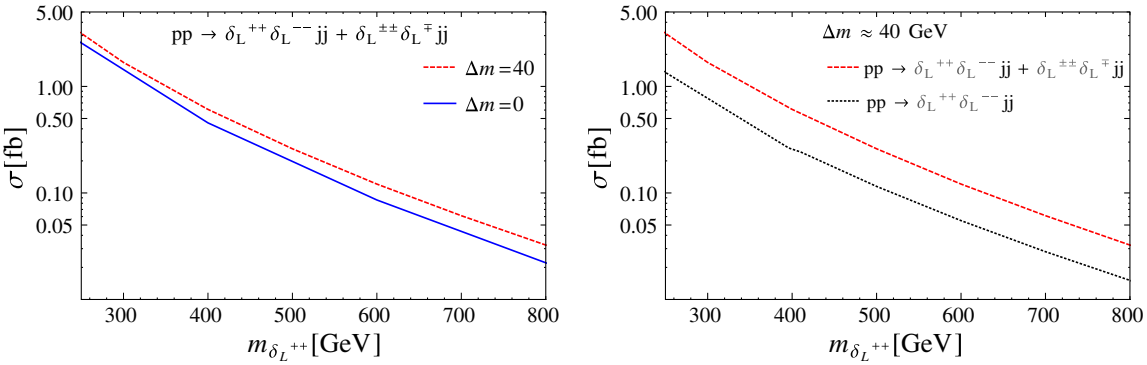

FIG. 2 (color online). Left: Cross section for $pp \to \delta_L^{++}\delta_L^{--}jj + \delta_L^{\pm\pm}\delta_L^{\mp}jj$ at LHC14 for different values of Δm, where $\Delta m = m_{\delta_L^{++}} - m_{\delta_L^{+}}$. Right: Comparison of the production cross sections for $pp \to \delta_L^{++}\delta_L^{--}jj$ and $pp \to \delta_L^{++}\delta_L^{--}jj + \delta_L^{\pm\pm}\delta_L^{\mp}jj$ at LHC14, keeping $\Delta m \approx 40$ GeV fixed for all $m_{\delta_L^{\pm\pm}}$.

B. Decay of the doubly charged Higgs boson

Here we will show that with $v_L = 0$, δ_L^{++} dominantly decays to a pair of like-sign leptons (e, μ, τ) that can give rise to an unique collider signature. Since the B-L charge is 2 for the triplet, their Yukawa couplings are given by the Lagrangian

$$\mathcal{L}_Y = ih_{ij}^M \psi_{iL}^T \mathcal{C}\tau_2 \Delta_L \psi_{jL} + \text{c.c.}, \tag{15}$$

where i, j are the lepton generation indices, and $\mathcal{C}$ is the charge conjugation operator. ψ_L is the left-handed lepton doublet. Various constraints may arise on the Yukawa couplings from different experiments. These constraints on h_{ij}^M have been discussed in great detail in Refs. [13,36,41]. Here we only list the relevant ones for our study.

The Bhaba scattering yields a constraint [41] on h_{ee}^M,

$$(h_{ee}^M)^2 \lesssim 9.7 \times 10^{-6} \left(\frac{m_{\delta_L^{++}}}{\text{GeV}}\right)^2. \tag{16}$$

The muon $g-2$ receives a contribution from the δ_L^{++} [36,42]. Using the current measurement, $\Delta a_\mu = a_\mu^{\text{exp}} - a_\mu^{\text{SM}} = 288 \times 10^{-11}$ [40], we obtain

$$(h_{\mu\mu}^M)^2 \lesssim 1.5 \times 10^{-5} \left(\frac{m_{\delta_L^{++}}}{\text{GeV}}\right)^2. \tag{17}$$

From the upper limit of $\text{BR}(\mu \to e\gamma)$ [40,41], we get

$$h_{ee}^M \cdot h_{\mu\mu}^M \lesssim 5.8 \times 10^{-5} \left(\frac{m_{\delta_L^{++}}}{\text{GeV}}\right)^2. \tag{18}$$

The nondiagonal coupling $h_{\mu e}^M$ can break the lepton number of each generation and is the most stringently constrained [36,40]. Between the first two generations, we find

$$h_{\mu e}^M \cdot h_{ee}^M \lesssim 2 \times 10^{-11} \left(\frac{m_{\delta_L^{++}}}{\text{GeV}}\right)^2. \tag{19}$$

Finally, no constraint on $h_{\tau\tau}^M$ is available yet.

$\Delta L = 2$ decay rates into different flavor combinations depend on the relative strength of the Yukawa couplings h_{ij}^M. In this paper we consider two sample cases: (i) $\text{BR}(\delta_L^{++} \to e^+e^+) = 50\%$, $\text{BR}(\delta_L^{++} \to \mu^+\mu^+) = 50\%$, and (ii) $\text{BR}(\delta_L^{++} \to \tau^+\tau^+) = 100\%$. For case (i), we assume a diagonal h_{ij}^M.

As $v_L = 0$, the decay processes $\delta_L^{++} \to W^+W^+$ and $\delta_L^{++} \to \delta_L^+\delta_L^+$ are forbidden. The constraints on the mass splittings rule that the decays $\delta_L^{++} \to \delta_L^+ W^+$, $\delta_L^{++} \to \delta_L^+\delta_L^+\delta_L^0$ and $\delta_L^{++} \to W^+W^+\delta_L^0$ can only occur virtually. These virtual decays have a subdominant branching ratio compared to that of the dilepton decay channel; hence, we ignore them in this paper.

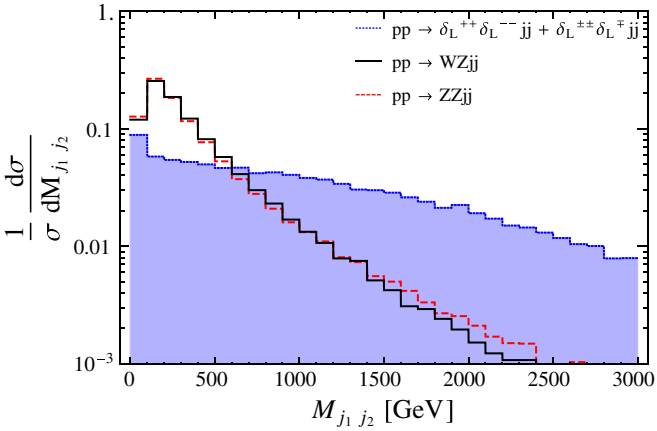

FIG. 3 (color online). Distribution of the dijet invariant mass $M_{j_1 j_2}$ normalized to unity for the tagging jet pair (j_1, j_2) for the signal and all the backgrounds before the VBF cuts are applied. The signal is inclusive of the processes $\delta_L^{++}\delta_L^{--}jj$ and $\delta_L^{\pm\pm}\delta_L^{\mp}jj$ for the benchmark point $(m_{\delta_L^{++}}, m_{\delta_L^{+}}) = (460\ \text{GeV}, 420\ \text{GeV})$ at $\sqrt{s} = 14$ TeV. The tagged jets (j_1, j_2) are the pair of jets with largest dijet invariant mass among all final-state jet pairs. j_1 and j_2 have been sorted among themselves by their p_T.

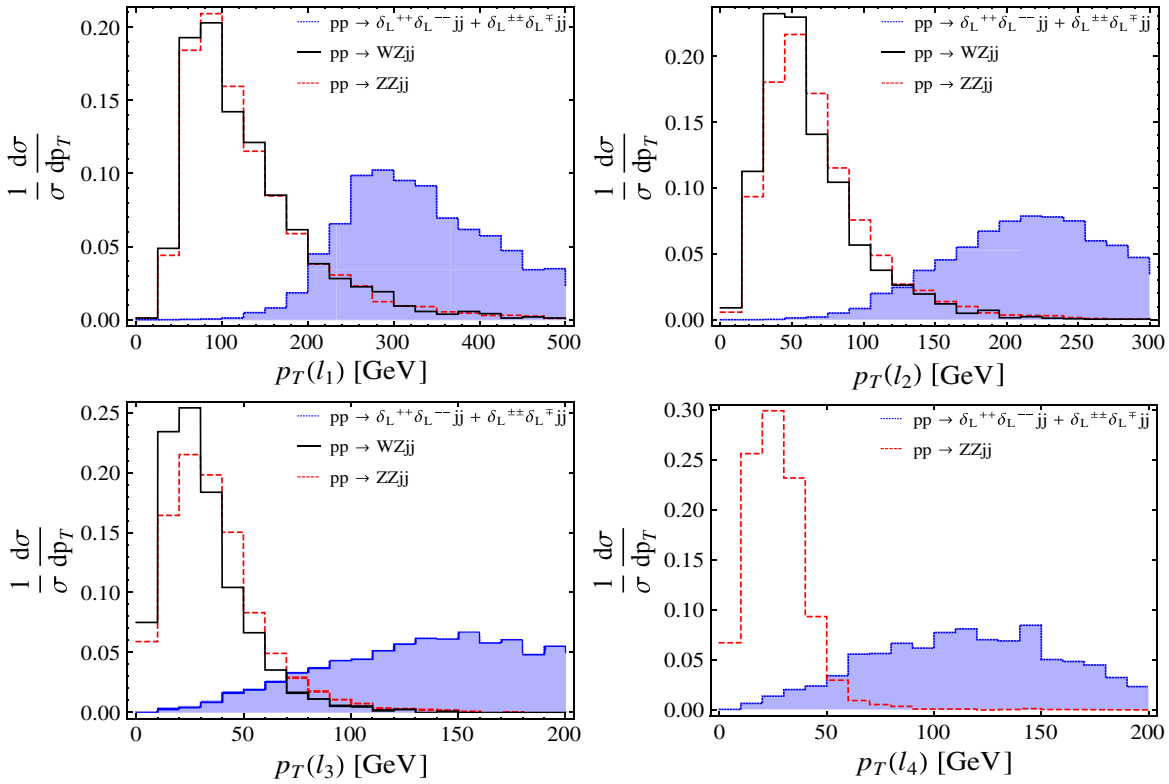

FIG. 4 (color online). p_T distribution of the leptons, normalized to unity, in the $\geq 3l+ \geq 2j$ final state for the signal $[(m_{\delta_L^{++}}, m_{\delta_L^{+}}) = (460\ \text{GeV}, 420\ \text{GeV})]$ and SM backgrounds at $\sqrt{s} = 14$ TeV.

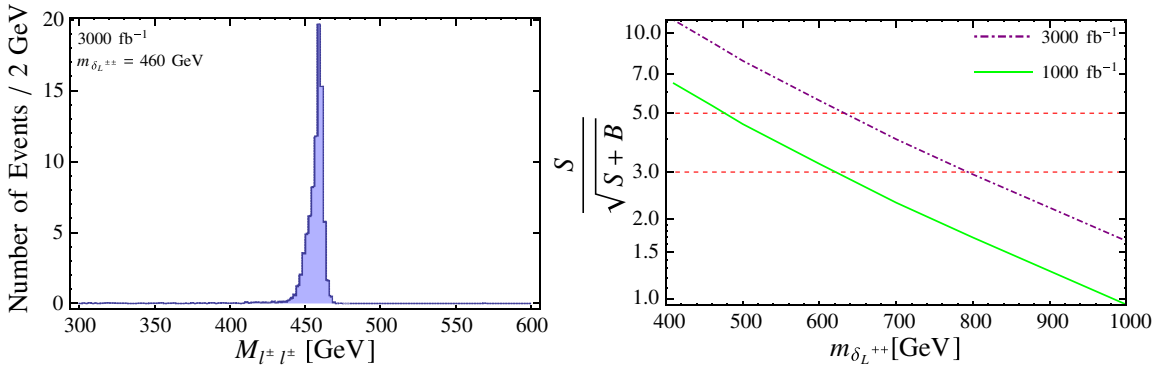

FIG. 5 (color online). Left: The signal invariant mass distribution of like-sign dilepton pairs in the $\geq 3l+ \geq 2j$ final state, after applying all the kinematic cuts. Since the number of background events drops to less than 1 after all the cuts, they have not been included in this figure. Right: The significance curves assume 1000 fb^{-1} (solid) and 3000 fb^{-1} (dot-dashed) LHC luminosities at 14 TeV. The 3σ and 5σ levels are shown as horizontal lines, and Δm is kept at $\approx$40 GeV.

TABLE I. Summary of the signal and background cross sections and the corresponding statistical errors at our chosen benchmark point, after each kinematical cut in the light lepton decay scenario. The LHC energy is 14 TeV.

$(m_{\delta_L^{++}}, m_{\delta_L^{+}})$ [GeV]	Selection cuts	Signal [fb]	ZZjj [fb]	WZjj [fb]
(460, 420)	Basic cuts	0.1540 ± 0.0011	585.9 ± 1.4	3513 ± 8
	VBF	0.0403 ± 0.0005	39.98 ± 0.36	211.8 ± 2.1
	≥ 3 leptons	0.0317 ± 0.0005	0.2131 ± 0.0028	1.702 ± 0.033
	lepton p_T cuts	0.0301 ± 0.0005	0.0126 ± 0.0007	0.1015 ± 0.0080
	Z veto	0.0291 ± 0.0005	0.0005 ± 0.0001	0.0057 ± 0.0019
	δ_L^{++} mass window	0.0285 ± 0.0005	0.0001 ± 0.0001	0.0002 ± 0.0002

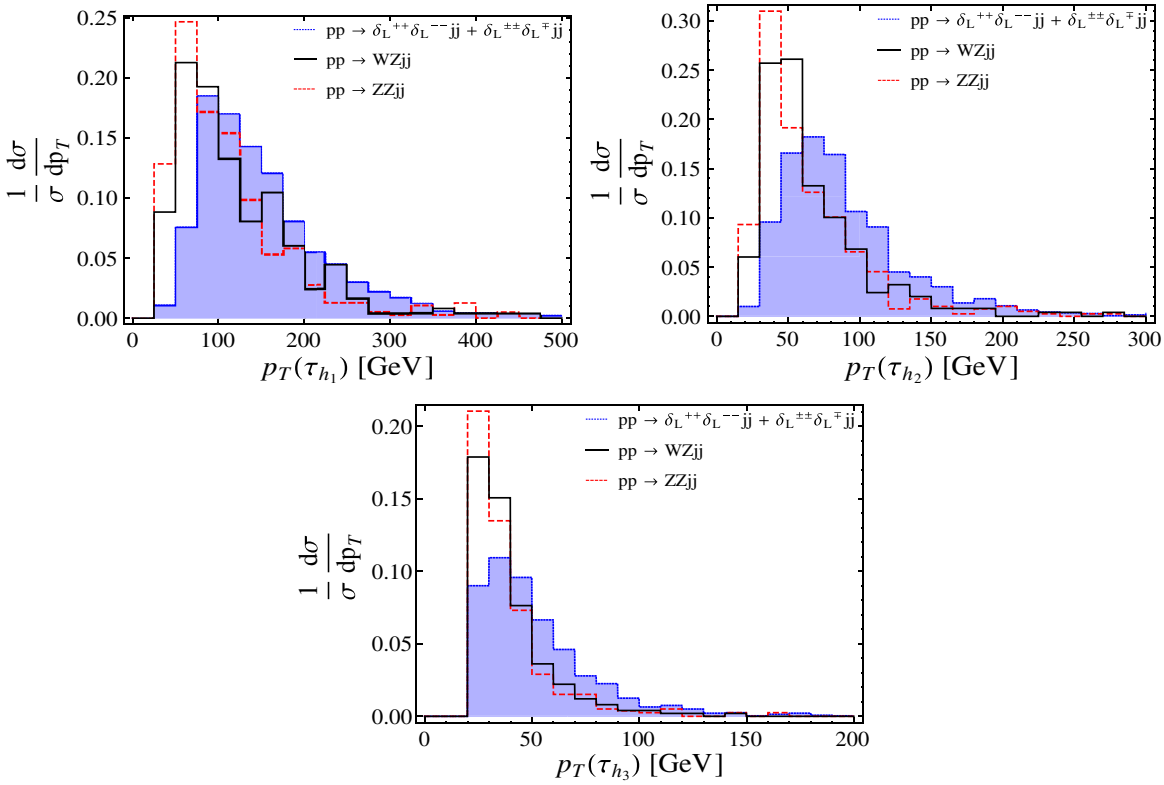

FIG. 6 (color online). p_T distribution of the τ_hs, normalized to unity, in the $\geq 3\tau_h + \geq 2j + E_{\rm T}$ final state for the signal $[(m_{\delta_L^{++}}, m_{\delta_L^{+}}) = (210\ \text{GeV}, 170\ \text{GeV})]$, as well as SM backgrounds at $\sqrt{s} = 14$ TeV. For all the plots, the τ ID efficiency and jet $\to \tau_h$ fake rate are considered to be 70% and 2%, respectively.

IV. RESULTS

Here we present the significance of a potential LHC signal from the two $\delta_L^{\pm\pm}$ decay scenarios, $\delta_L^{\pm\pm} \to l^{\pm} l^{\pm}$ $(ll = 50\%ee, 50\%\mu\mu)$ and $\delta_L^{\pm\pm} \to \tau^{\pm}\tau^{\pm}(100\%)$. The L-R symmetric model is implemented with the FeynRules v1.7.200 [43] package. The signal and background events are generated using MADGRAPH5 [44], followed by showering and hadronization by PYTHIA [45] and the detector simulation by PGS4 [46].

A. Like-sign light lepton pairs

We first consider the decay of $\delta_L^{\pm\pm}$ into like-sign light lepton pairs (e, μ). The production processes $pp \to \delta_L^{\pm\pm}\delta_L^{\mp} jj$ and $pp \to \delta_L^{++}\delta_L^{--} jj$ lead to a final state of at least three leptons $(\geq 3l)$ and two or more jets $(\geq 2j)$.

The CMS analysis [30] has set the latest bound on $m_{\delta_L^{\pm\pm}}$ from the three-lepton channel to be 444 GeV for a 100% decay to ee and 459 GeV for a 100% decay into $\mu\mu$. The corresponding bounds for four-lepton final states are 382 GeV for ee and 395 GeV for $\mu\mu$. In comparison, the ATLAS bound [32] for the $\geq 3e/\mu$ channel is 330 GeV, and their bounds from the four-lepton channel [13,31] are 409 GeV and 398 GeV for ee and $\mu\mu$, respectively.

The major SM backgrounds for our final state are $pp \to WZjj$ and $pp \to ZZjj$. The kinematic cuts imposed to reduce these background are as follows:

(1) *Basic cuts:* The signal and background events are preselected with the requirement of at least two jets with $p_{Tj} > 30$ GeV and $|\eta_j| < 5$. The subsequent cuts applied on the preselected events are optimized to maximize the signal significance, $S/\sqrt{S+B}$,

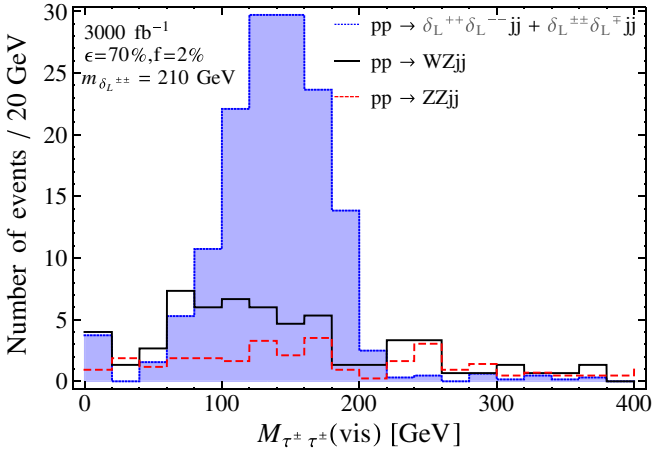

FIG. 7 (color online). The visible mass of the like-sign τ_h pair for the signal (dotted) and backgrounds (solid and dashed) for the $\geq 3\tau_h + \geq 2j + E_{\rm T}$ final state, after all the kinematic cuts. $(m_{\delta_L^{++}}, m_{\delta_L^{+}}) = (210\,\text{GeV}, 170\,\text{GeV})$, with $\epsilon = 70\%$ and $f = 2\%$ at 14 TeV.

TABLE II. Summary of the effective cross sections and the corresponding statistical errors of both the signal and the backgrounds after each cut is applied in the τ decay scenario at $\sqrt{s} = 14$ TeV.

$(m_{\delta_L^{++}}, m_{\delta^+})$ [GeV]		Selection cuts	Signal [fb]	ZZjj [fb]	WZjj [fb]
		Basic cuts	2.222 ± 0.009	585.9 ± 1.4	3513 ± 8
		VBF cuts	0.4655 ± 0.0040	39.98 ± 0.36	211.8 ± 2.1
(210, 170)	$\epsilon = 50\%$, $f = 1\%$	≥ 3 τ_h's	0.0196 ± 0.0008	0.0038 ± 0.0007	0.0138 ± 0.0028
		$\tau_h p_T$ cuts	0.0147 ± 0.0007	0.0016 ± 0.0005	0.0070 ± 0.0021
		E_{T} cut	0.0120 ± 0.0006	0.0011 ± 0.0004	0.0048 ± 0.0016
	$\epsilon = 70\%$, $f = 2\%$	≥ 3 τ_h's	0.0487 ± 0.0013	0.0068 ± 0.0009	0.0364 ± 0.0051
		$\tau_h p_T$ cuts	0.0356 ± 0.0006	0.0032 ± 0.0007	0.0168 ± 0.0034
		E_{T} cut	0.0292 ± 0.0010	0.0020 ± 0.0005	0.0112 ± 0.0027

where S and B denote signal and background rates, respectively.

(2) *VBF cuts:* Denoting j_1, j_2 to be the pair of jets with the highest M_{jj}, we require (i) $p_T(j_1), p_T(j_2) > 50$ GeV, (ii) $\eta_{j_1} * \eta_{j_2} < 0$, (iii) $|\Delta\eta_{j_1,j_2}| > 4$, and (iv) $M_{j_1 j_2} > 500$ GeV. We find from Fig. 3 that the $M_{j_1 j_2}$ of the backgrounds fall below those of the signal above 500 GeV.[2]

(3) ≥ 3 *leptons:* At least three light leptons ($l = e, \mu$) with $p_T(l) > 10$ GeV and $|\eta_l| < 2.5$. This cut reduces the background by a factor of 10^{-2} due to the low $W \to l\nu$ and $Z \to ll$ branching fractions.

(4) *Lepton p_T cuts:* The p_T distribution of the leptons of the signal and the backgrounds is shown in Fig. 4. The figure clearly shows that the leptons arising from $\delta_L^{\pm\pm}$ decay are more energetic than the leptons coming from W, Z bosons. This allows us to impose stringent p_T cuts on the leptons as follows: $p_T(l_1) > 120$ GeV, $p_T(l_2) > 100$ GeV, $p_T(l_3) > 50$ GeV, and $p_T(l_4) > 30$ GeV. These cuts are instrumental to reducing backgrounds by an order of magnitude.

(5) *Z veto:* An opposite-sign dilepton invariant mass, $|M_{l^+l^-} - m_Z| > 10$ GeV, removes the $ZZjj$ background effectively.

(6) *δ_L^{++} mass window cut:* Like-sign dilepton invariant mass, $|M_{l^\pm l^\pm} - m_{\delta_L^{++}}| < 10\% m_{\delta_L^{++}}$.

The reconstructed invariant mass of the like-sign dilepton pairs after all the cuts is shown in Fig. 5 for $m_{\delta_L^{++}} = 460$ GeV. One can readily observe the distribution peaks sharply at $m_{\delta_L^{\pm\pm}}$. Table I gives the signal and background cross sections after applying each cut. The significances ($S/\sqrt{S+B}$) have been plotted in Fig. 5 as a function of $m_{\delta_L^{++}}$, keeping Δm fixed at ~40 GeV, for upcoming LHC luminosities at 1000 fb^{-1} and 3000 fb^{-1}. We find that at the 3σ (5σ) level, the $m_{\delta_L^{++}}$ can be probed up to 620 (480) GeV for 1000 fb^{-1} luminosity, and up to 800 (640) GeV for 3000 fb^{-1}.

[2]For all the figures presented in this paper, the signal and background kinematic distributions are not stacked.

B. Like-sign tau pairs

In this subsection, we shall present the VBF search strategy in the multi-τ final state. The search with τ leptons is the most difficult amongst the three generations of leptons because of low τ identification efficiency at the LHC. The τ lepton tagging requires the τ to decay hadronically, denoted by "τ_h." Similarly to the light lepton case, the signal final state contains $\geq 3\tau_h + \geq 2j$ together with E_{T}. Existing CMS bounds [30] for the $\tau\tau$ final state (for the DY process) are 204 GeV and 169 GeV in the three- and four-lepton channels, respectively. ATLAS does not offer a limit for this scenario.

Tagging the τ_h involves the τ_h identification (ID) ϵ and the fake rate f coming from jets. We look at the case $\epsilon = 50\%$, $f = 1\%$, with both ϵ and f flat over $p_T > 20$ GeV [47], and an alternative enhanced efficiency at $\epsilon = 70\%$, which could be achievable in future LHC searches [48], with a higher fake rate $f = 2\%$.[3] The kinematical cuts imposed are listed as follows:

(1 and 2) *Basic and VBF cuts:* Same as in the light lepton case (see Sec. IV A). The rest of the cuts are similarly optimized to maximize the signal significance, $S/\sqrt{S+B}$.

(3) ≥ 3 *tagged* τ_h: We have selected events with at least three τ_h's in the final state with $p_T(\tau_h) > 20$ GeV and $\eta(\tau_h) < 2.3$, which are required [47] for our assumed ϵ and f.

(4) *$\tau_h p_T$ cuts:* Since a τ loses part of its p_T as E_{T}, illustrated in Fig. 6, we use softer p_T cuts: $p_T(\tau_{h_1}) > 50$ GeV, $p_T(\tau_{h_2}) > 50$ GeV, and $p_T(\tau_{h_3}) > 30$ GeV, and no p_T cut for additional τ_hs. This cut achieves a 75% cut

[3]PGS4, by default, has a τ_h identification (ID) efficiency (ϵ) of 30%–40%. To study the impact on this search due to τ_h ID performance, an object reconstructed by visible particles from the hadronic decay of τ in PYTHIA is used at a rate of ID efficiency (50% or 70%). Correspondingly, each PGS4 jet object is misidentified as a τ_h object at a probability of 1% or 2% (fake rate f in the text).

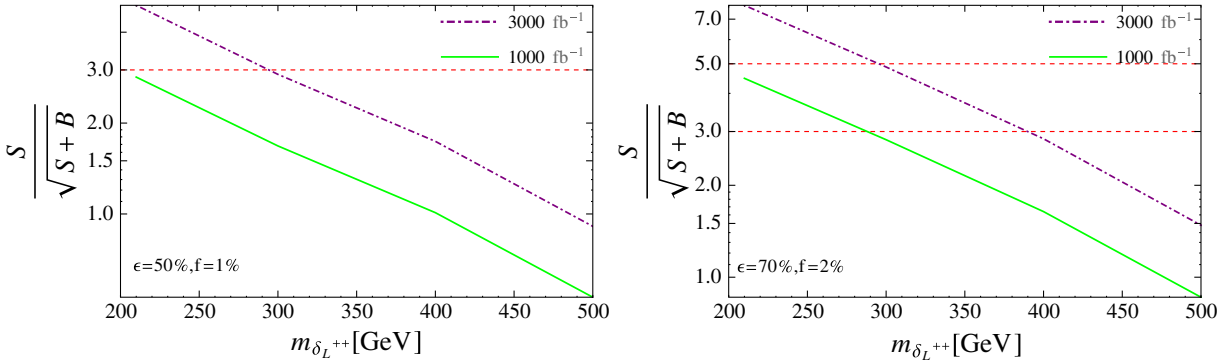

FIG. 8 (color online). The τ_h channel significance versus $m_{\delta_L^{++}}$ for τ_h ID efficiency $\epsilon = 50\%$ with the jet fake rate $f = 1\%$ (left panel) and for $\epsilon = 70\%$, $f = 2\%$ (right panel). The LHC energy is 14 TeV, and Δm is kept at 40 GeV. The significances for luminosities at 1000 and 3000 fb^{-1} are plotted as solid and dot-dashed curves, respectively.

efficiency for the signal and reduces the background by a factor of 2.

(5) E_{T} *cut:* $E_{\mathrm{T}} > 50$ GeV.

Because the τ decays into the invisible ν_τ, the invariant mass of the like-sign τ pair cannot be reconstructed completely. Figure 7 shows the visible mass, $M_{\tau^\pm\tau^\pm}(\mathrm{vis})$, of the like-sign τ_h pair from $m_{\delta^{++}} = 210$ GeV. Due to the loss of visible p_T, the $\tau\tau$ mass shows a broad distribution that centers at 140 GeV, below the parent δ_L^{++} mass.

The signal and background cross sections are listed in Table II. The signal significance is plotted as a function of $m_{\delta_L^{++}}$ in Fig. 8, where we keep $\Delta m = m_{\delta_L^{++}} - m_{\delta_L^{+}} = 40$ GeV. For a 3000 fb^{-1} luminosity at 14 TeV, $m_{\delta_L^{++}}$ can be probed up to 300 GeV at 3σ with $\epsilon = 50\%$, $f = 1\%$. With enhanced tagging rates ($\epsilon = 70\%$, $f = 2\%$), the δ_L^{++} mass reach goes up to 390 GeV and the corresponding discovery (5σ) limit of $m_{\delta_L^{++}}$ is 300 GeV. With 1000 fb^{-1} data, however, the 3σ limit is 290 GeV for $\epsilon = 70\%$ and $f = 2\%$.[4]

V. CONCLUSION

In this paper, we investigated the LHC prospects of pair production of the doubly charged Higgs bosons from L-R symmetric models via the VBF process. The VBF offers a complementary search strategy to the existing studies on the DY process and can be important in understanding the electroweak origin of the doubly charged Higgs boson.

We chose the $v_L = 0$ scenario to avoid Z-boson decay into $\delta_L^0 \delta_L^{0*}$, which is invisible. Due to the constraint from ρ_{EW}, the $\delta_L^{++}, \delta_L^{+}$ mass splitting is less than $\sim$40 GeV, and δ_L^{++} dominantly decays into like-sign lepton pairs. The LHC signature consists of multiple (≥ 3) leptons, two tagging jets in the forward region of the detector, and missing energy (in the τ_h final state only). Due to different identification efficiencies, we studied the light lepton (e, μ) and hadronically decaying τ_h scenarios separately.

A series of kinematical cuts, led by the VBF topological cuts, the number of leptons in the final state, and p_T cuts, are found to be effective against SM backgrounds. For a luminosity of 1000 fb^{-1}, we can set an 3σ exclusion limit up to 620 GeV for the light lepton final state and 290 GeV for the τ_h final state. The latter assumes a τ_h ID efficiency of 70% and a 2% jet fake rate. For 3000 fb^{-1} luminosity, we achieved an exclusion limit at $m_{\delta_L^{++}} \sim 800$ GeV and 390 GeV in the light lepton (e, μ) and τ_h final states.

ACKNOWLEDGMENTS

We thank Kechen Wang, Alfredo Gurrola, Sanjay Padhi, Goran Senjanovic, Francisco del Aguila, and Olivier Mattelaer for helpful discussions. We would also like to thank Youngdo Oh for reading the manuscript. This work is supported in part by DOE Grant No. DE-FG02-13ER42020 and the World Class University (WCU) project through the National Research Foundation (NRF) of Korea funded by the Ministry of Education, Science, and Technology (Grant No. R32-2008-000-20001-0). T. K. is also supported in part by the Qatar National Research Fund under Project No. NPRP 5-464-1-080. Y. G. is supported by Mitchell Institute for Fundamental Physics and Astronomy.

APPENDIX A: THE HIGGS-SECTOR GENERAL POTENTIAL OF THE LEFT-RIGHT MODEL

The potential of the scalar sector of the model we have studied, following Refs. [36,37], is given by

[4]The V + jets production (where $V = W, Z$), however, could be a considerable source of the background in large jet multiplicity environments at the LHC where the jet-to-τ_h-fake rate is at a level of 1%–2%. A full analysis, which takes into account all the fake backgrounds using DELPHES 3 [49] as the detector simulator will be performed in a forthcoming study [50] motivated by the type II seesaw mechanism for neutrino mass generation.

$$V = -\mu_1^2 \mathrm{Tr}\phi^\dagger\phi + \lambda_1(\mathrm{Tr}\phi^\dagger\phi)^2 + \lambda_2 \mathrm{Tr}\phi^\dagger\phi\phi^\dagger\phi + \frac{1}{2}\lambda_3(\mathrm{Tr}\phi^\dagger\tilde{\phi} + \mathrm{Tr}\tilde{\phi}^\dagger\phi)^2 + \frac{1}{2}\lambda_4(\mathrm{Tr}\phi^\dagger\tilde{\phi} - \mathrm{Tr}\tilde{\phi}^\dagger\phi)^2$$
$$+ \lambda_5 \mathrm{Tr}\phi^\dagger\phi\tilde{\phi}^\dagger\tilde{\phi} + \frac{1}{2}\lambda_6(\mathrm{Tr}\phi^\dagger\tilde{\phi}\phi^\dagger\tilde{\phi} + \mathrm{Tr}\tilde{\phi}^\dagger\phi\tilde{\phi}^\dagger\phi) - \mu_2^2(\mathrm{Tr}\Delta_L^\dagger\Delta_L + \mathrm{Tr}\Delta_R^\dagger\Delta_R)$$
$$+ \rho_1[(\mathrm{Tr}\Delta_L^\dagger\Delta_L)^2 + (\mathrm{Tr}\Delta_R^\dagger\Delta_R)^2] + \rho_2(\mathrm{Tr}\Delta_L^\dagger\Delta_L\Delta_L^\dagger\Delta_L + \mathrm{Tr}\Delta_R^\dagger\Delta_R\Delta_R^\dagger\Delta_R) + \rho_3(\mathrm{Tr}\Delta_L^\dagger\Delta_L)(\mathrm{Tr}\Delta_R^\dagger\Delta_R)$$
$$+ \rho_4(\mathrm{Tr}\Delta_L\Delta_L\mathrm{Tr}\Delta_R^\dagger\Delta_R^\dagger + \mathrm{Tr}\Delta_L^\dagger\Delta_L^\dagger\mathrm{Tr}\Delta_R\Delta_R) + \alpha_1\mathrm{Tr}\phi^\dagger\phi(\mathrm{Tr}\Delta_L^\dagger\Delta_L + \mathrm{Tr}\Delta_R^\dagger\Delta_R)$$
$$+ \alpha_2(\mathrm{Tr}\Delta_R^\dagger\phi^\dagger\phi\Delta_R + \mathrm{Tr}\Delta_L^\dagger\phi\phi^\dagger\Delta_L) + \alpha_2'(\mathrm{Tr}\Delta_R^\dagger\tilde{\phi}^\dagger\tilde{\phi}\Delta_R + \mathrm{Tr}\Delta_L^\dagger\tilde{\phi}\tilde{\phi}^\dagger\Delta_L), \quad \text{(A1)}$$

where $\tilde{\phi} \equiv \tau_2\phi^*\tau_2$. $\tau_i/2$ is the usual 2×2 representation matrix of $SU(2)$. One should note that additional discrete symmetries, $\Delta_L \to \Delta_R$, $\Delta_R \to -\Delta_R$, and $\phi \to i\phi$ have been imposed in addition to L-R symmetry, to have $v_L = 0$ at the natural minima of the potential [36]. As has been already mentioned in Eq. (4), we have defined a combination of parameters appearing in the above Higgs potential as

$$\rho_{\mathrm{dif}} \equiv \rho_3 - 2(\rho_2 + \rho_1),$$
$$\Delta\alpha \equiv (\alpha_2 - \alpha_2')/2. \quad \text{(A2)}$$

The mass spectrum of the left Higgs triplet, obtained after minimizing the above potential, has been discussed below. We have neglected terms of order v_L/v_R here.

The left-handed doubly charged Higgs boson δ_L^{++} is a physical mass eigenstate itself with mass

$$m^2_{\delta_L^{++}} = \frac{1}{2}\rho_{\mathrm{dif}}v_R^2 - \rho_2 v_L^2 + \Delta\alpha\kappa_1^2. \quad \text{(A3)}$$

The physical singly charged Higgs boson is

$$\tilde{\delta_L^+} = \frac{\delta_L^+ + \frac{\sqrt{2}v_L}{\kappa_1}\phi_2^+}{\left(1 + \frac{2v_L^2}{\kappa_1^2}\right)^{1/2}} \quad \text{(A4)}$$

with mass

$$m^2_{\delta_L^+} = \frac{1}{2}\rho_{\mathrm{dif}}v_R^2 + \frac{1}{2}\Delta\alpha(\kappa_1^2 + 2v_L^2). \quad \text{(A5)}$$

The neutral Higgs sector consists of two pure states δ_L^0 and δ_L^{0*}, which have the same mass:

$$m^2_{\delta_L^0} = m^2_{\delta_L^{0*}} = \frac{1}{2}\rho_{\mathrm{dif}}v_R^2. \quad \text{(A6)}$$

The complete set of mass eigenstates of the Higgs sector of the L-R model is discussed in Refs. [36,37]. The results presented above are valid for the both VEV scenarios under consideration. We can obtain the formulas for relevant cases by simply recalling the fact that for $v_L \neq 0$, $\rho_{\mathrm{dif}} = 0$, while for $v_L = 0$, ρ_{dif} can be varied. Thus, we can readily observe that in the second scenario, δ_L^+ is also a pure mass eigenstate.

APPENDIX B: THE FEYNMAN RULES FOR THE LEFT HIGGS TRIPLET–GAUGE INTERACTION

We have presented the Feynman rules for the interaction of the vector bosons and the left Higgs triplet scalars in Table III.

TABLE III. Feynman rules for the interaction of the vector bosons and the left Higgs triplet scalars of the L-R symmetric model. Here p_i stands for the 4-momentum of the ith particle at the vertex, with the convention that all the particle momenta are coming into the vertex. For brevity, $\cos 2\theta_W$ has been abbreviated as c_{2W}.

Vertex	Feynman rule
$\gamma_\mu\gamma_\nu\delta_L^+\delta_L^-$	$2ig^2s_W^2g_{\mu\nu}$
$\gamma_\mu\gamma_\nu\delta_L^{++}\delta_L^{--}$	$8ig^2s_W^2g_{\mu\nu}$
$\gamma_\mu\delta_L^+\delta_L^-$	$igs_W(p_2-p_3)_\mu$
$\gamma_\mu\delta_L^{++}\delta_L^{--}$	$2igs_W(p_2-p_3)_\mu$
$\gamma_\mu\delta_L^0\delta_L^-W_\nu^+$	$ig^2s_Wg_{\mu\nu}$
$\gamma_\mu\delta_L^+\delta_L^{--}W_\nu^+$	$-3ig^2s_Wg_{\mu\nu}$
$\gamma_\mu\delta_L^-W_\nu^+$	$ig^2s_Wv_Lg_{\mu\nu}/\sqrt{2}$
$\delta_L^0\delta_L^-W_\mu^+$	$ig(p_1-p_2)_\mu$
$\delta_L^+\delta_L^{--}W_\mu^+$	$-ig(p_1-p_2)_\mu$
$\delta_L^0\delta_L^{--}W_\mu^+W_\nu^+$	$-2ig^2g_{\mu\nu}$
$\delta_L^{--}W_\mu^+W_\nu^+$	$-i\sqrt{2}g^2v_Lg_{\mu\nu}$
$\delta_L^0\delta_L^{0*}W_\mu^+W_\nu^-$	$ig^2g_{\mu\nu}$
$\delta_L^+\delta_L^-W_\mu^+W_\nu^-$	$2ig^2g_{\mu\nu}$
$\delta_L^{++}\delta_L^{--}W_\mu^+W_\nu^-$	$ig^2g_{\mu\nu}$
$\delta_L^0W_\mu^+W_\nu^-$	$ig^2v_Lg_{\mu\nu}/\sqrt{2}$
$\gamma_\mu\delta_L^{++}\delta_L^{--}Z_\nu$	$4ig^2s_Wc_{2W}g_{\mu\nu}/c_W$
$\gamma_\mu\delta_L^+\delta_L^-Z_\nu$	$-2ig^2s_W^3g_{\mu\nu}/c_W$
$\delta_L^0\delta_L^-W_\mu^+Z_\nu$	$-ig^2(1+s_W^2)g_{\mu\nu}/c_W$
$\delta_L^+\delta_L^{--}W_\mu^+Z_\nu$	$-ig^2(1-3s_W^2)g_{\mu\nu}/c_W$
$\delta_L^-W_\mu^+Z_\nu$	$-ig^2v_L(1+s_W^2)g_{\mu\nu}/(\sqrt{2}c_W)$
$\delta_L^0\delta_L^{0*}Z_\mu Z_\nu$	$2ig^2g_{\mu\nu}/c_W^2$
$\delta_L^{++}\delta_L^{--}Z_\mu Z_\nu$	$2ig^2c_{2W}^2g_{\mu\nu}/c_W^2$
$\delta_L^+\delta_L^-Z_\mu Z_\nu$	$2ig^2s_W^4g_{\mu\nu}/c_W^2$
$\delta_L^0Z_\mu Z_\nu$	$i\sqrt{2}g^2v_Lg_{\mu\nu}/c_W^2$
$\delta_L^0\delta_L^{0*}Z_\mu$	$-ig(p_1-p_2)_\mu/c_W$
$\delta_L^+\delta_L^-Z_\mu$	$-igs_W^2(p_1-p_2)_\mu/c_W$
$\delta_L^{++}\delta_L^{--}Z_\mu$	$igc_{2W}(p_1-p_2)_\mu/c_W$

[1] J. C. Pati and A. Salam, Phys. Rev. D **10**, 275 (1974); **11**, 703(E) (1975).
[2] R. N. Mohapatra and J. C. Pati, Phys. Rev. D **11**, 566 (1975).
[3] G. Senjanovic and R. N. Mohapatra, Phys. Rev. D **12**, 1502 (1975).
[4] R. N. Mohapatra and G. Senjanovic, Phys. Rev. Lett. **44**, 912 (1980).
[5] H. Georgi and M. Machacek, Nucl. Phys. **B262**, 463 (1985).
[6] N. Arkani-Hamed, A. G. Cohen, E. Katz, and A. E. Nelson, J. High Energy Phys. 07 (2002) 034.
[7] P. H. Frampton, Phys. Rev. Lett. **69**, 2889 (1992).
[8] F. Pisano and V. Pleitez, Phys. Rev. D **46**, 410 (1992).
[9] F. del Aguila and M. Chala, J. High Energy Phys. 03 (2014) 027.
[10] F. del Aguila, M. Chala, A. Santamaria, and J. Wudka, Eur. Phys. J. Web Conf. **60**, 17002 (2013).
[11] V. Rentala, W. Shepherd, and S. Su, Phys. Rev. D **84**, 035004 (2011).
[12] F. del Aguila, M. Chala, A. Santamaria, and J. Wudka, Phys. Lett. B **725**, 310 (2013).
[13] N. Quintero, Phys. Rev. D **87**, 056005 (2013).
[14] S. Kanemura, K. Yagyu, and H. Yokoya, Phys. Lett. B **726**, 316 (2013).
[15] G. Bambhaniya, J. Chakrabortty, J. Gluza, M. Kordiaczynska, and R. Szafron, J. High Energy Phys. 05 (2014) 033.
[16] A. G. Akeroyd and C.-W. Chiang, Phys. Rev. D **80**, 113010 (2009).
[17] A. G. Akeroyd, C.-W. Chiang, and N. Gaur, J. High Energy Phys. 11 (2010) 005.
[18] M. D. Tonasse, Phys. Lett. B **718**, 86 (2012).
[19] A. Cagil and H. Dag, arXiv:1203.2232.
[20] A. G. Akeroyd and H. Sugiyama, Phys. Rev. D **84**, 035010 (2011).
[21] M. Aoki, S. Kanemura, and K. Yagyu, Phys. Rev. D **85**, 055007 (2012).
[22] E. J. Chun and P. Sharma, J. High Energy Phys. 08 (2012) 162.
[23] H. Sugiyama, K. Tsumura, and H. Yokoya, Phys. Lett. B **717**, 229 (2012).
[24] T. Han, B. Mukhopadhyaya, Z. Si, and K. Wang, Phys. Rev. D **76**, 075013 (2007).
[25] G. Azuelos, K. Benslama, and J. Ferland, J. Phys. G **32**, 73 (2006).
[26] C.-W. Chiang, T. Nomura, and K. Tsumura, Phys. Rev. D **85**, 095023 (2012).
[27] C. Englert, E. Re, and M. Spannowsky, Phys. Rev. D **88**, 035024 (2013).
[28] S. Godfrey and K. Moats, Phys. Rev. D **81**, 075026 (2010).
[29] B. Grinstein, C. W. Murphy, D. Pirtskhalava, and P. Uttayarat, J. High Energy Phys. 05 (2014) 083.
[30] S. Chatrchyan *et al.* (CMS Collaboration), Eur. Phys. J. C **72**, 2189 (2012).
[31] G. Aad *et al.* (ATLAS Collaboration), Phys. Rev. D **85**, 032004 (2012).
[32] G. Aad *et al.* (ATLAS Collaboration), Phys. Rev. D **87**, 052002 (2013).
[33] R. N. Mohapatra and G. Senjanovic, Phys. Rev. D **23**, 165 (1981).
[34] C. S. Lim and T. Inami, Prog. Theor. Phys. **67**, 1569 (1982).
[35] F. I. Olness and M. E. Ebel, Phys. Rev. D **32**, 1769 (1985).
[36] J. F. Gunion, J. Grifols, A. Mendez, B. Kayser, and F. I. Olness, Phys. Rev. D **40**, 1546 (1989).
[37] N. G. Deshpande, J. F. Gunion, B. Kayser, and F. I. Olness, Phys. Rev. D **44**, 837 (1991).
[38] Y. Zhang, H. An, X. Ji, and R. N. Mohapatra, Nucl. Phys. **B802**, 247 (2008).
[39] A. Maiezza, M. Nemevsek, F. Nesti, and G. Senjanovic, Phys. Rev. D **82**, 055022 (2010).
[40] J. Beringer *et al.* (Particle Data Group), Phys. Rev. D **86**, 010001 (2012).
[41] K. Huitu, J. Maalampi, A. Pietila, and M. Raidal, Nucl. Phys. **B487**, 27 (1997).
[42] F. S. Queiroz and W. Shepherd, Phys. Rev. D **89**, 095024 (2014).
[43] N. D. Christensen and C. Duhr, Comput. Phys. Commun. **180**, 1614 (2009).
[44] J. Alwall, M. Herquet, F. Maltoni, O. Mattelaer, and T. Stelzer, J. High Energy Phys. 06 (2011) 128.
[45] T. Sjostrand, S. Mrenna, and P. Z. Skands, J. High Energy Phys. 05 (2006) 026.
[46] PGS4 is a parameterized detector simulator. We use version 4 from http://www.physics.ucdavis.edu/~conway/research/software/pgs/pgs4-general.htm.
[47] CMS Collaboration, Report No. CMS-PAS-TAU-11-001, available at http://cds.cern.ch/record/1337004.
[48] CMS Collaboration, Tau Performance Plots for 2012, available at https://twiki.cern.ch/twiki/bin/view/CMSPublic/PhysicsResultsPFT.
[49] J. de Favereau, C. Delaere, P. Demin, A. Giammanco, V. Lemaître, A. Mertens, and M. Selvaggi (DELPHES 3 Collaboration), J. High Energy Phys. 02 (2014) 057.
[50] B. Dutta, T. Ghosh, T. Kamon, and S. Padhi (to be published).